A study of positronium formation in anodic alumina

2008 J. Phys.: Condens. Matter 20 095206

(http://iopscience.iop.org/0953-8984/20/9/095206)

J. Phys.: Condens. Matter **20** (2008) 095206 (8pp) doi:10.1088/0953-8984/20/9/095206

A study of positronium formation in anodic alumina

N Djourelov[1,2,8], C A Palacio[3], J De Baerdemaeker[3], C Bas[1], N Charvin[1], K Delendik[4], G Drobychev[5,6], D Sillou[5], O Voitik[4] and S Gninenko[7]

[1] LMOPS, University of Savoie, Bâtiment IUT, 73376 Le Bourget-du-lac Cedex, France
[2] Institute for Nuclear Research and Nuclear Energy, 72 Tzarigradsko Chaussee, BG-1784 Sofia, Bulgaria
[3] Department of Subatomic and Radiation Physics, Ghent University, 86 Proeftuinstraat, B-9000 Gent, Belgium
[4] Institute of Electronics, 22 Logoiski Trakt, BY-220090 Minsk, Belarus
[5] LAPP-University of Savoie, BP 110, F74941 Annecy-le-Vieux, France
[6] Institute for Nuclear Problems, 11, Bobruiskaya Street, BY-220030 Minsk, Belarus
[7] Institute for Nuclear Research, 7a, 60th October Anniversary Avenue, 117312 Moscow, Russia

E-mail: nikdjour@inrne.bas.bg

Received 31 October 2007, in final form 17 January 2008
Published 8 February 2008
Online at stacks.iop.org/JPhysCM/20/095206

Abstract

Al_2O_3 samples grown with natural well-ordered channels (having sizes of 30–90 nm in diameter) perpendicular to the surface, one side closed, were measured by means of Doppler broadening (DB) by variable energy positron (VEP) beam and positron annihilation lifetime (PAL) spectroscopy. The samples annealed at 300 and 560 °C showed amorphous structure and no positronium (Ps) formation. The sample annealed at 850 °C showed γ-phase polycrystalline structure and Ps formation. We were not able to prove from the PAL spectroscopy results themselves whether Ps is confined to the channels. We discuss the results of decomposition of the DB annihilation peak into four Gaussians. We conclude that the greater Ps fraction is confined to the channels. From the Compton-to-peak ratio analysis, the fraction of all the injected positrons which form o-Ps and in this form escape from the sample (for a VEP experiment, we have e^+ injected from the open side of the channels) has been estimated as being ∼20%.

(Some figures in this article are in colour only in the electronic version)

1. Introduction

Charge, parity, time reversal (CPT) symmetry is one of the most important laws of field theory. It states that the physical properties are invariant when one simultaneously changes the signs of the charge and of the spatial and time coordinates of particles. There are theoretical attempts to develop models which violate the CPT theorem. Study of antimatter properties would help in proving or rejecting the CPT theorem. Antihydrogen is the first synthesized antiatom in a series of experiments (for a review see [1]). It has been produced by interactions of positrons with an antiproton beam. It was suggested that an antihydrogen beam can be produced by interaction of a cold antiproton beam with cloud of positronium (Ps) atoms [2]. Ps is easily formed by positron (e^+) interactions in some porous or low electron density materials. In the case of high pore interconnectivity a great number of Ps will find a way to escape to the vacuum [3]. Also, on the surface of different materials bombarded with slow positrons with energies of up to few keV, fast Ps can be produced. Fast (10–100 eV) Ps is formed from backscattered or epithermal positrons by electron capture on the surface [4].

Van Petegem *et al* have demonstrated the power of Doppler broadening (DB) studies using a variable energy positron beam and for the first time the authors succeeded in

[8] Author to whom any correspondence should be addressed.

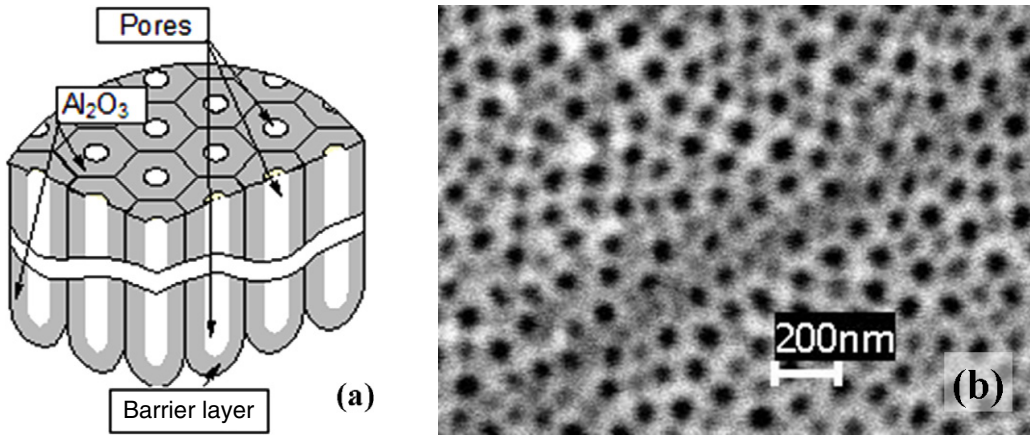

Figure 1. (a) Schematic representation of anodic alumina structure and (b) electron microscopy image of the surface of anodic Al_2O_3.

obtaining estimations of the diffusion lengths of e^+ and Ps separately [5]. Their experiments showed that in the bulk of single-crystalline Al_2O_3 and MgO, Ps is not formed but Ps emission from the surface has been observed. A subject of special interest has been vitreous α-SiO_2. In the last case Ps is being formed in the bulk and at very low energy of the incident e^+ about 55% of them are converted into Ps emitted from the surface [5]. However, for the proposed antihydrogen experiment the Ps cloud should be cold and that is why researchers are looking for a material in which Ps is formed in the bulk and at the same time a great part of it can escape.

Anodic Al_2O_3 is known to be grown with well-ordered porosity (regularly distributed channels perpendicular to the direction of growth) [6]. Ps has been detected as localized in the intercrystalline spaces of polycrystalline Al_2O_3 powder [7, 8]. Thus the well-ordered channel porosity combined with Ps formation in the bulk in anodic Al_2O_3 samples would eventually lead to high Ps yield and Ps emission into vacuum. In this study we applied several positron annihilation techniques to anodic alumina in order to try to investigate Ps yield and sites of Ps confinement.

2. Experimental details

2.1. Samples

Samples were formed by electrochemical oxidation of aluminum in electrolytes, weakly dissolving alumina, and consist of regular hexagonally packed cells, which are parallel to each other and perpendicular to the surface of the aluminum substrate. Every cell includes an axial pore, closed by a barrier oxide layer on the side of the aluminum anode (figure 1). The cell diameter of anodic alumina samples is mainly defined by the anodization voltage. The thickness of the barrier layer may vary from 10 nm to 1 μm. The details of porous alumina production technology are described elsewhere [9].

Some of the sample characteristics are reported in table 1. The samples are split into two groups. The first group (I) includes samples annealed at 300 °C for 2 h with different diameters of the channels, while the second group (II) includes samples with same size channels annealed at different temperatures.

Table 1. Labels, thickness d, channel diameter D, annealing temperature t, and density of the sample ρ.

Sample	d (mm)	D (nm)	t (°C)	ρ (g cm^{-3})
I30D	0.1	30	300	1.15
I50D	0.113	50	300	1.26
I80D	0.093	80	300	1.29
II300t	0.091	60	300	1.24
II560t	0.089	60	560	1.28
II850t	0.0885	60	850	1.25

2.2. Conventional positron annihilation spectroscopy

For positron annihilation lifetime (PAL) experiments a positron source was prepared by depositing about 0.9 MBq of aqueous ^{22}NaCl on a 7 μm thick Kapton foil having a 15 × 15 mm^2 area. After drying, the foil was covered with a foil of the same size, glued on the edges with epoxy resin. A sandwich arrangement (sample–source–sample) was used. In order to ensure full stopping of emitted e^+, stacks of three sample slabs plus a Si slab were used on each side to form the source–sample sandwich. PAL experiments were carried out using a conventional fast–fast coincidence system (time to amplitude converter (TAC) range 50 ns, 0.025 ns/channel) having a time resolution of FWHM = 230 ps (full width at half-maximum). The measurements were carried out in a vacuum chamber at a moderate vacuum and at room temperature. Sequences of 6–15 spectra for every sample were recorded every 30 min with total counts in individual spectra of $\sim 3 \times 10^5$. A rough preliminary analysis was performed to monitor possible e^+ irradiation effects. Such an effect was not found. For each type of sample the spectra were summed together, resulting in a statistics of $>2 \times 10^6$ counts. The contribution to the lifetime spectrum of the source was estimated to be 12% (0.382 ns) and annihilation in Si to be ∼5% (0.219 ns). Both contributions were treated as source corrections in the final analysis of the summed spectra by the LT v.9 program [10]. When Ps was detected the analyses were performed with the assumption that

Table 2. Lifetimes and corresponding intensities obtained by discrete exponential component analysis of the PAL sample.

Sample	τ_1 (ns)	τ_2 (ns)	I_1 (%)	I_2 (%)	$\tau_{p\text{-}Ps}$ (ns)	$\tau_{o\text{-}Ps1}$ (ns)	$\tau_{o\text{-}Ps2}$ (ns)	$I_{p\text{-}Ps}$ (%)	$I_{o\text{-}Ps1}$ (%)	$I_{o\text{-}Ps2}$ (%)
I30D	0.303(1)	0.587(4)	81.8(5)	18.2(5)						
I50D	0.312(2)	0.566(9)	82.5(9)	17.5(9)						
I80D	0.303(1)	0.564(2)	80.7(6)	19.3(1)						
II300t	0.300(2)	0.575(2)	80.9(3)	19.1(2)						
II560t	0.298(2)	0.588(7)	80.9(7)	19.1(7)						
II850t	0.225(3)	0.519(9)	59.1(9)	25.8(9)	0.125	3.02(6)	33.5(5)	3.8(1)	3.7(1)	7.6(2)
II850t[a]	0.225	0.519	54.3(3)	22.4(2)	0.125	4.7(1)	75.9(6)	5.8(1)	3.3(1)	14.1(1)

[a] Results obtained from the PAL spectrum taken with TAC range 500 ns.

the para-positronium (p-Ps) lifetime is $\tau_{p\text{-}Ps} = 0.125$ ns and the ratio of p-Ps intensity to ortho-positronium (o-Ps) intensity is $I_{p\text{-}Ps}/\Sigma I_{o\text{-}Ps} = 1/3$. In all reported PAL analyses the variance of the fit was better than 1.2.

2.3. Doppler broadening study using a variable energy positron beam

The energy spectra were recorded every 30 min (statistics of 3×10^5 counts in the 511 keV region) for incident positron energies (E_{e^+}) from 0.1 to 20 keV and were carried out with a Canberra high purity Ge detector (HPGe) with a resolution FWHM = 1.17 keV at the 514 keV line of ^{85}Sr on the slow e^+ beam at Ghent. The HPGe detector was coupled to a digital signal processor unit, model 2060 from Canberra. The detector was set up aside and perpendicular to the direction of incident e^+ at the position of the sample. Two experiments were performed with sample II850t. For the experiment O45, the sample was oriented with the open side of the channels and its surface at an angle of 45° to the beam and to the detector. For the second experiment C45, with the same sample, the geometry was the same as for experiment O45 but with the closed side of the channel to the beam.

More details about the geometry of such an experiment can be found elsewhere [11]. The DB 511 keV lines were analyzed with a sum of up to four Gaussians by using the DBAN program (Matlab based software for decomposition of the Doppler broadened annihilation line into Gaussians. Available on request).

For all of the PAL and DB experiments the samples were annealed at 200 °C in vacuum for 2 h prior to the measurements in order to remove the probable moisture absorbed during the sample storage in air.

3. Results

3.1. Conventional positron annihilation lifetime spectroscopy

The most commonly accepted method of analyzing of PAL spectra is called discrete exponentials analysis and it suggests that e^+ annihilate from states with well-defined annihilation (decay) rates $\lambda = 1/\tau$. The results for the lifetime spectra are summarized in table 2. All the spectra with only one exception (II850t) are resolved into only two exponentials with lifetimes $\tau_1 \approx 0.3$ ns (∼81%) and $\tau_2 \approx 0.57$ ns (∼19%). The x-ray analysis has shown that the as-grown samples have amorphous structure. Similar short lifetimes have been reported for amorphous alumina powder; however, the authors have found a long lifetime of ∼1.5 ns (10%) which is attributed to o-Ps pick-off annihilation [8]. That is why for our samples the short lifetimes may be associated with e^+ annihilation in the bulk material and the longer ones may be interpreted as relating to e^+ trapped at internal surfaces of inner particle voids. After injection into the material the e^+ is quickly thermalized and at the end of its track may pick up an e^- from its own spur (terminal cloud of secondary e^-) to form Ps. The Ps formation probability depends not only on the available free volume but also on e^- and e^+ scavengers (radicals, ions, dipoles due to different impurities introduced into the structure during growth) and e^- and e^+ mobility. The fact that all the samples show comparable porosity (see ρ in table 1 and compare with the crystalline alumina density of $\rho_{cr} = 4.2$ g cm^{-3}) leads to two possible explanations of the fact that Ps is not formed in all the samples, except for II850t. The first possibility is that some ions from the acids used are captured in the structure and inhibit the Ps formation by e^+ and/or e^- scavenging. The second explanation is that the e^+ and e^- mobility is very low. The fact that in a powder of amorphous Al_2O_3 microparticles about 10% o-Ps is observed leads us to the conclusion that the first possibility has a stronger influence on the present samples.

As can be seen in table 1, the samples studied (except for II850t) display rather constant lifetimes and corresponding intensities. Two conclusions can be drawn. From the results for group I it follows that the process of sample growth is well reproducible and from group II it follows that annealing up to 560 °C does not significantly change the sample structure. The latter is in excellent agreement with the differential scanning calorimetry (DSC), x-ray diffraction (XRD) and thermogravimetric analysis (TGA) shown in figures 2 and 3.

The aim of the DSC, XRD and TGA measurements (figures 2 and 3) was to study phase transition processes of anodic alumina structures produced in different technological conditions. Two different kinds of samples were chosen for measurements: samples of 'type 1' were produced in oxalic acid, having channels of 50–70 nm diameters; and samples of 'type 2' were produced in phosphoric acid, having channels of 140–160 nm. The samples were scanned from room temperature to 1200 °C under oxygen atmosphere.

To interpret the results obtained we compared them with aluminum oxide phase transition data. According to published information, amorphous alumina makes a transition to the γ-phase at a temperature in the region from 300 to 600 °C. At

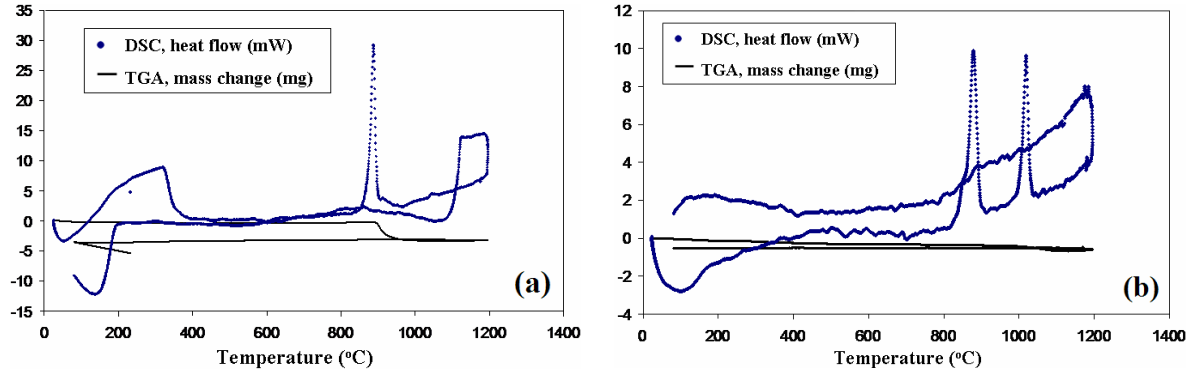

Figure 2. DSC and thermogravimetric analysis of anodic alumina samples produced in (a) oxalic acid (type 1) and (b) phosphoric acid (type 2).

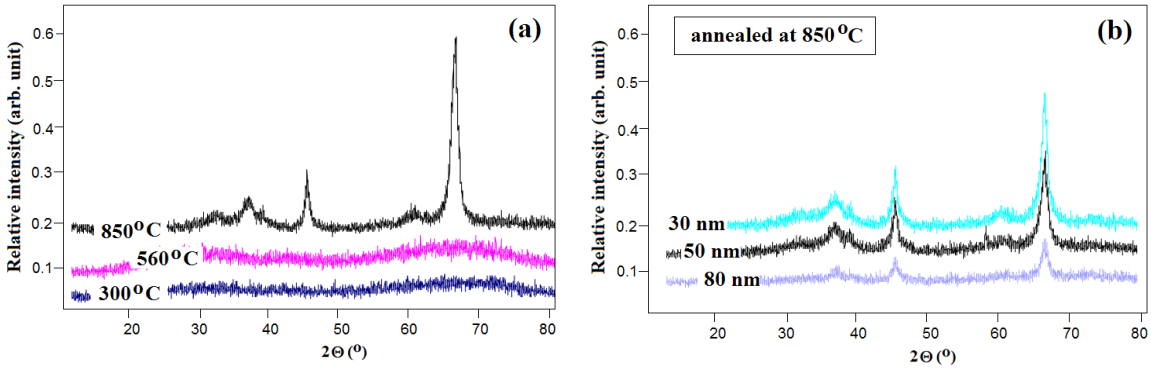

Figure 3. XRD analysis for: (a) samples with 60 nm diameter of the channels (the results are representative for the other diameters 30, 50, 80 nm, as well) annealed at different temperatures and (b) samples with different diameters of the channels annealed at 850 °C.

about 850 °C, alumina makes a phase transition from the γ-phase to the δ-phase which in turn makes a transition to the Θ-phase at 1050 °C. After 1200 °C, the Θ-phase is changed to stable α-phase.

As one can see in figure 2, detected peaks of the phase transition may correspond to this γ-phase to δ-phase transition and to the subsequent transition of δ-phase to Θ-phase or to a direct transition from γ-phase to Θ-phase. However, it should be noted that the measured temperatures of these phase transitions are slightly (less than 30 °C) different from those indicated in the literature for pure anodic alumina material [12–14]. But, due to technological factors, the structure of the samples reported here contains some quantity of acid residues, water, and impurities. Molecules of acid residues can enter into traps of the alumina structure and cannot be removed. Water molecules in anodic alumina material can form boehmite (aluminum hydroxyl). All these inclusions can modify the crystalline structure, which causes a change of phase transition temperature.

The presence of these inclusions also may be responsible for the mass modification during phase transitions. At 880 °C this effect cannot be explained by water loss. Reduction of mass of the 'type 1' samples is probably caused by losses of CO_2 from traps. Samples of 'type 2' were produced in phosphoric acid and contain P_2O_5 residuals which have larger size, so they cannot exit from traps and remain in intercrystalline areas.

Tests of some samples by XRD methods were carried out. The results are presented in figure 3. As one can see in figure 3(a), a significant formation of polycrystalline gamma phase is observed only after an annealing at 850 °C. Figure 3(b) shows the results of XRD studies for the samples with different (30, 50 and 80 nm) diameters of channels, annealed at 850 °C.

We can conclude that the results are in good agreement with published ones [13–15]. The reported measurements have shown that the processes of phase transition in the samples studied are rather complex and depend on the growth conditions. A significant change in the sample structure occurs when the sample is annealed at 850 °C. Obviously, crystallization takes place. The present studies show the presence of γ-phase in all samples annealed at 850 °C (see figure 3(b)).

Shantarovich *et al* have shown significant differences between powders (microparticle size of ∼100 nm) of amorphous and of polycrystalline α-phase Al_2O_3 not only in the o-Ps intensities but also in their lifetimes [8]. On the basis of kinetic equations describing the formation of non-localized Ps followed by diffusion and trapping into free volume holes and the size of the amorphous particles, the authors concluded that due to the low diffusion coefficient in amorphous alumina, non-localized Ps does not reach the surface of the microparticles and the observed o-Ps lifetime of 1.5 ns comes from pick-off annihilation of o-Ps confined in

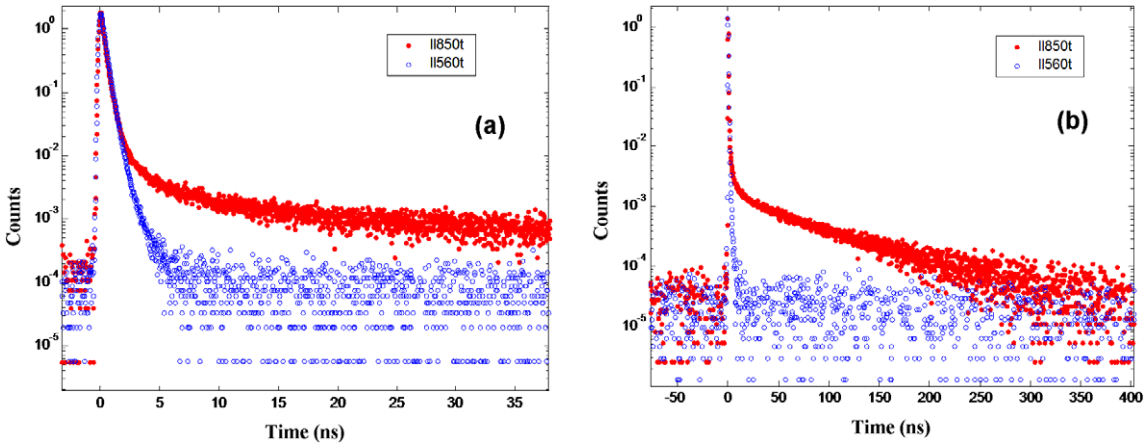

Figure 4. Comparison of the lifetime spectra for samples II560t and II850t after background subtraction: (a) 50 ns TAC range, (b) 500 ns TAC range.

voids within the microparticles. The diffusion constant of non-localized Ps is greatly increased in the crystalline phase and the long lifetime reported by Shantarovich *et al* of 42.4 ns (4.2%) is due to pick-off annihilation of o-Ps localized in the space between the microparticles. The latter is confirmed in the study of Van Petegem *et al*, who have found that the o-Ps diffusion length of 15 nm for vitreous α-SiO_2 is two times longer than that for e^+ [5].

Special attention has to be paid when there is a component in a lifetime spectrum which does not decay completely within the chosen TAC range of the PAL spectrometer, as is the case for sample II850t (see figure 4(a); the background is not reached at the end of the timescale). The spectra shown in figure 4(b) have been measured with ten times longer TAC range (500 ns, 0.25 ns/channel). The discrete lifetime analysis for sample II850t gives rather different results for the long lifetimes (see table 2). For lifetimes longer than 10 ns the extended Tao–Eldrup model (ETE) has to be applied to convert the o-Ps pick-off lifetime to the size of the pores [15, 16]. The lifetime $\tau_{o-Ps1} = 4.7$ ns may be associated with small free volumes with the radius of 0.5 nm within or between the crystalline grains. The observed lifetime $\tau_{o-Ps2} = 75.9$ ns corresponds to the following sizes of the pores: $R = 3.1$ nm assuming spherical shape and $r = 2.3$ nm assuming cylindrical shape. The pore sizes determined in such a way cannot be associated with the channels of 60 nm diameter for which we should measure a lifetime of 135 ns according to the ETE model. The density of $\rho_b \approx 2.5$ for the Al_2O_3 bulk material between the channels was obtained using the rough estimation that 50% of the sample volume consists of channels (see figure 1) and using the sample density given in table 1. The estimated density ρ_b is considerably lower than that of crystalline alumina ρ_{cr}. This means that there is a significant free volume fraction in the bulk material between the channels. If Ps were to annihilate in these free volumes (between the grains of the polycrystalline material) the size would be $R = 3.1$ nm. However, due to the long e^+ and Ps diffusion lengths in crystalline Al_2O_3 it seems unlikely that Ps would be confined between the grains without escaping to the channels.

As one can see from the electron microscopy image (figure 1) the distances between the channels are of the same order as the channel widths. The structures of the powder of α-alumina and sample II850t (γ-phase) are crystallographically different, but both forms are polycrystalline and probably can be considered analogous according to the distances between free spaces, e^+ and non-localized Ps diffusion lengths, i.e. the longest lifetime should come mainly from pick-off annihilation of o-Ps localized within the channels.

A theory exists which considers that Ps is initially formed by some excess energy and is slowly thermalized [17]. A description of the model (called elastic thermalization lifetime analysis, ETLA) can be found in the help for LT v.9 [10] or [17]. The model assumes: (a) Ps is created as a weakly bound pair, e^-–e^+, and the initial contact density (η), i.e. the initial electron density on the positron divided by the density in the ground state of Ps, is $\eta(0) < 1$; (b) gradually, because of the slowing down, the pair is more and more localized and η increases. The localization process influences the Ps pick-off lifetime, which changes from a low value $\tau_{o\text{-}Ps}(0)$ to a higher value $\tau_{o\text{-}Ps}(\infty)$, i.e. $1/\tau_{o\text{-}Ps}(t) = 1/\tau_{o\text{-}Ps}(\infty) + [1/\tau_{o\text{-}Ps}(0) - 1/\tau_{o\text{-}Ps}(\infty)]\exp(-\gamma t)$, where γ is the rate of the thermalization process. Simultaneously, the intrinsic lifetime of Ps decreases, due to the increasing of η.

Because the ETE model considers a thermalized o-Ps and as a consequence of the ETLA model, it follows that the pore radius has to be estimated from the asymptotic o-Ps lifetime $\tau_{o\text{-}Ps}(\infty)$.

Our attempts to apply the ETLA model of LT v.9 to the suggestion of one site for o-Ps annihilation showed that $\tau_{o\text{-}Ps}(\infty) \approx 149$ ns. Although this value slightly exceeds the intrinsic o-Ps lifetime (142 ns), it is indicated that by slow thermalization we may explain the discrepancy between the longest lifetime obtained by the discrete lifetime analysis and the expected lifetime of 135 ns as estimated from the channel size using the ETE model.

In the case of two localization sites for o-Ps between the grains in the bulk and in the channels the model became too complicated and we have not succeeded in getting a reasonable ETLA fit to this suggestion. Hence, by means of

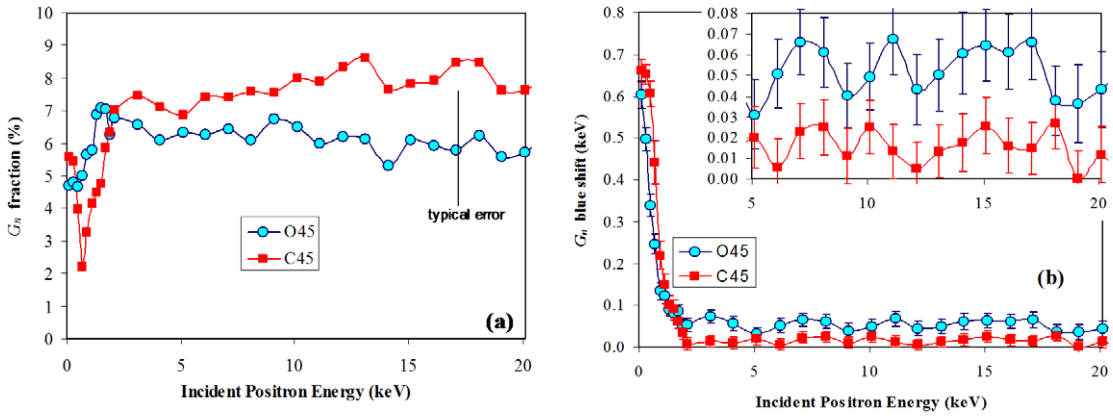

Figure 5. Narrow Gaussian fraction (a) and shift (b) versus incident positron energy, E_{e^+}, as a result of a decomposition of the Doppler annihilation line into three Gaussians for experiments O45 (open side of the channels, 45° to the beam axis), C45 (closed side of the channels, 45° to the beam axis), performed on sample II850t. The intrinsic FWHM of G_n (not plotted) behaves in a similar way to the shift, starting from ∼0.6 keV at the lowest E_{e^+}, and saturates at ∼0 keV at higher E_{e^+}. The lines are to guide the eye.

PAL measurements we are not able to confirm or reject the possibility of two localization sites.

3.2. Doppler broadening study using a variable energy positron beam

We followed the same idea as is reported in [5] but with a different geometry, described in detail in [11]. First we analyzed the DB annihilation line for both experiments O45 and C45, suggesting for the fitting curve three Gaussians without any constraint. The middle and broad Gaussians were obtained centered with almost constant widths, intrinsic (obtained after accounting for the HPGe resolution), with FWHM $= 2.50 \pm 0.03$ and 4.63 ± 0.03 keV. The middle Gaussian is attributed to e^+ and pick-off o-Ps annihilation with valence e^-, while the broad one is attributed to e^+ annihilation with core e^-. The fraction of the narrow Gaussian G_n and its shift are presented in figure 5. The intrinsic FWHM of G_n (not plotted) behaves in similar way to the shift, starting from ∼0.6 keV at the lowest E_{e^+} and saturating at ∼0 keV at higher E_{e^+}. The saturation fraction of p-Ps at high E_{e^+} is ∼6–8% which, within the error limit, agrees satisfactorily with the p-Ps fraction of 5.8% obtained from PAL measurements (see table 2).

Actually, in such analyses for samples in which bulk Ps is formed, the narrow Gaussian has a complex contribution from p-Ps which is formed on the surface (p-Ps^s) and escapes from the sample and p-Ps formed in the bulk. Surface emission of p-Ps^s is well studied [5, 11] for several polymers and oxides, including single-crystalline α-Al_2O_3, and in all cases the Gaussian which corresponds to p-Ps^s has been reported as having FWHM of ≈0.7 keV and a shift of ∼0.6 keV, and these parameters are independent of E_{e^+}. The G_n parameters at the lowest e^+ energy for O45 and C45 when the bulk p-Ps yield is negligible are in perfect agreement with the reported ones. The C45 experiment shows the saturation level of the G_n shift at 0.02 keV. In this experiment, asymmetry of the DB line is not expected at high E_{e^+} due to the barrier layer which closes the channels and makes the mean normal to the surface component of p-Ps momentum zero. The fact that at the saturation level the G_n is not exactly centered is a result of the non-perfect background subtraction around the annihilation line. For the experiment O45 the G_n shift is 0.06, being higher than that for C45 by 0.04 keV. If we consider Ps as thermalized, its velocity will be $v = 7 \times 10^4$ m s^{-1} (this is an underestimation because the Ps confinement is not taken into account). So, the p-Ps mean path will be $> v\tau_{\text{p-Ps}} = 875$ nm, which is comparable to the channel lengths (see table 1). Consequently, a fraction of p-Ps will reach the open side of the channels and after escaping they will not be subjected any longer to collisions with the channel wall. Another fraction which has a momentum component toward the bottom of the channels will collide with the bottom, changing the component direction toward the surface. Both effects will contribute to the component of p-Ps momentum normal to the surface which will not be compensated. The extra G_n shift at high E_{e^+} cannot be explained if Ps is localized and annihilates between the grains in the bulk Al_2O_3 and does not reach the channels.

We have analyzed C45 and O45 data using four Gaussians, i.e. splitting G_n into two Gaussians by fixing the width FWHM $= 0.7$ keV and shift to 0.6 keV of the Gaussian which corresponds to p-Ps^s and using a centered Gaussian for the second narrow one. The intrinsic FWHM of the second one was obtained from the fit close to 0 keV. Figure 6 depicts the fractions of these two narrow Gaussians at low E_{e^+}. For the experiment C45 the incident e^+ at very low energies are stopped within the barrier layer which capes the channels. At $E_{e^+} = 0.8$ keV we see an increase of the bulk p-Ps for C45 but not for O45. So, at this energy, e^+ can penetrate the barrier layer. This energy corresponds to a mean positron implantation depth $z_m = 11$ nm, calculated from $z_m = (40/\rho_b)E^{1.6}$ [18], which agrees fairly well with the thickness of the barrier layer. The very low fraction of p-Ps annihilating in the bulk for C45 at $E_{e^+} < 0.8$ keV means that the fraction of Ps which annihilates in the barrier material is very low. We fit an e^+ diffusion model [5] to the data for the surface p-Ps fraction of C45 for $E_{e^+} < 0.8$ keV and we obtained the positron diffusion length $L_+ = 14 \pm 1$ nm for in the barrier layer, i.e. for polycrystalline

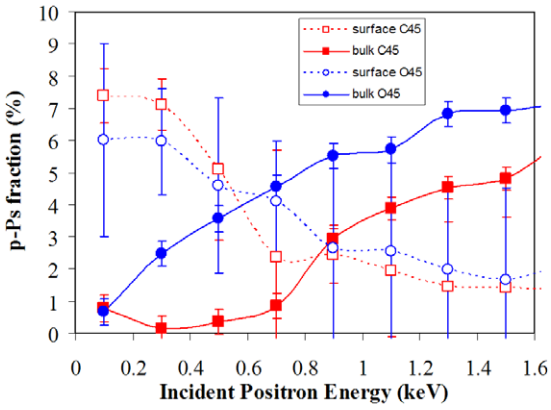

Figure 6. Fractions of the two narrow Gaussians which correspond to annihilation of p-Ps escaping from the surface (blue-shifted at 0.6 keV, intrinsic FWHM = 0.7 keV) and p-Ps annihilating in the bulk (centered, intrinsic FWHM of ≈0 keV) for experiments C45 and O45, as a function of incident positron energy E_{e^+}. The lines are to guide the eye.

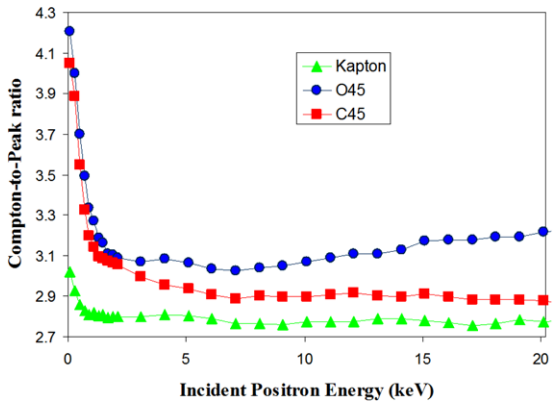

Figure 7. Compton-to-peak ratio, $R_{C/P}$, as a function of incident positron energy, E_{e^+}, for experiments O45 (open side of the channels, 45° to the beam axis), C45 (closed side of the channels, 45° to the beam axis) performed on sample II850t and for Kapton (127 μm thick, 45° to the beam axis).

γ-phase Al_2O_3. The last value is of the same order as that one obtained for single-crystalline Al_2O_3 and α-Al_2O_3 [5, 19]. Due to the fact that L_+ is of the same order of magnitude as the channel wall thickness (see figure 1(b)) we can draw the conclusion that most of the Ps reach the channels.

The classical meaning of the free path of a particle enclosed in a cavity is given by $l = 4V/S$, where V is the volume and S is the surface of the cavity. Thus, for a very long cylinder $l = D$, where $D = 60$ nm is the diameter of the channels. Consequently, o-Ps will be subjected to $v/l = 1.2 \times 10^4$ collisions per ns. The probability for o-Ps escaping from the one-side-open channel per collision is $p = (\pi D^2/4)/S = D/(4d) = 1.5 \times 10^{-5}$ (for the channel length $d \sim 10^5$ nm; see table 1). This means that o-Ps will escape from the channel if it decays after $l/(vp) =$ 6th ns. Simple calculation shows that for o-Ps with lifetime >76 ns more than 92% of the o-Ps decay after the sixth ns. The 92% estimation of o-Ps leaving the channels is underestimated for two reasons: first, part of the o-Ps decaying before the sixth ns will also escape, and second, the o-Ps velocity v is underestimated. Consequently, most of the o-Ps will escape from the channels.

The o-Ps which escapes from the sample will annihilate in the vacuum via 3γ annihilation, while the e^+ annihilation is mostly via 2γ annihilation (the 3γ positron annihilation cross section is only 1/372 of that for 2γ positron annihilation and can be neglected). If there is Ps formation there will be 3γ o-Ps annihilation with a fraction dependent on the o-Ps lifetime. The related $3\gamma/2\gamma$ annihilation ratio, known as the Compton-to-peak ratio ($R_{C/P}$, in our case defined as the counts in the region 150–450 keV divided by the counts in the 511 keV peak) is plotted as a function of incident positron energy, E_{e^+}, in figure 7. For comparison the $R_{C/P}$ for a Kapton film is plotted in figure 7, as well. In Kapton, Ps is not formed in the bulk and $R_{C/P}(E_{e^+} = 20 \text{ keV}) = 2.76$. For the same incident positron energy when the influence from the surface on $R_{C/P}$ is negligible, higher $R_{C/P}$ values are observed for experiment O45 compared to those for C45. The corresponding values of 3.19 and 2.89 are due to the 3γ annihilation of o-Ps.

Mills showed that the 3γ annihilation can be determined using the energy spectrum and calibration values for the counts in the 511 keV peak (P) and $R_{C/P}$ for two samples with 0 and 100% yield of 3γ annihilation [20]. The formula is easily modified if the second calibration sample has a known non-zero 3γ annihilation yield (f_k):

$$f = f_k \left[1 + \frac{P_k}{P_0} \frac{(R_k - R_f)}{(R_f - R_0)} \right]^{-1}, \qquad (1)$$

where the subscript k stands for the second calibration sample.

For the C45 experiment the 3γ annihilation fraction is due not to o-Ps escaping from the sample but to the large pore size. It can be estimated from $f_k = I_{o-Ps} \frac{\eta\lambda^0_{o-Ps}}{\eta\lambda^0_{o-Ps}+\tau^{-1}_{o-Ps}}$, where $\lambda^0_{o-Ps} = 1/142$ ns^{-1} is the rate of annihilation of o-Ps in vacuum. We may consider the contact density $\eta = 1$ due to the rather large space where Ps is localized, and using $\tau_{o\text{-}Ps} = 75.9$ ns (table 2) we obtain $f_k = 7.3\%$ for the suggestion $I_{o\text{-}Ps} = 21\%$ ($I_{o\text{-}Ps} = 3I_{p\text{-}Ps}$; $I_{p\text{-}Ps}$ is the G_n fraction of 7%, figure 6, at high E_{e^+}). From f_k, P and $R_{C/P}$ parameters for Kapton and C45, from equation (1) we obtain $f = 29.2$ for O45. Hence, $f - f_k = 22.0\%$ of the injected e^+ annihilate via 3γ o-Ps self-annihilation in the vacuum out of the sample, i.e. most of the formed o-Ps escape from the channels in vacuum.

4. Conclusions

We have measured PAL characteristics of Al_2O_3 samples grown with natural well-ordered channel porosity. For the samples with different channel diameters and annealed at temperatures up to 560 °C we found no variations in the e^+ lifetimes and, what is more important, no Ps formation. The lack of Ps formation has been explained by possible capture in the structure of ions from the acids used in the growth process. The only sample showing Ps formation is II850t which was annealed at 850 °C. On the basis of just PAL measurements,

we do not have any direct proof that Ps is trapped in the channels. However, there are two indications that the latter actually occurs. The first one is that the transformation into the polycrystalline form of alumina significantly increases the diffusion length of the non-localized Ps which, in this case, can easily reach the channels and be trapped there. The second indication is that the o-Ps components can be explained with one complex component according to the ETLA model and its asymptotic lifetime is close to the expected lifetime of o-Ps confined to the channels as estimated using the extended Tau–Eldrup model.

Doppler broadening experiments with a variable energy positron beam have been performed on sample II850t; the PAL measurements have shown Ps formation. From the decomposition of the DB 511 keV peak into four Gaussians for the C45 experiment we have found that there is no significant fraction of Ps confined within the matrix forming the channel walls, from which we are driven to the conclusion that Ps is localized in the channels. The Compton-to-peak ratio at high incident positron energy revealed an additional 3γ annihilation fraction for O45 compared to C45. The fraction of all the injected positrons which form o-Ps and escape the sample has been calculated as being $\sim$20%.

Acknowledgments

The first author (ND) wishes to thank CNRS, France for the support he received as a visiting scientist. G Drobychev wishes to thank the Ministry of National Education of France, Savoie University and the Belarusian Republican Foundation for Fundamental Research for their support. The authors are very grateful to Y Mugnier and M Lomello from ESIA for their help with preliminary thermogravimetry and AFM measurements. Finally the collaboration must acknowledge the support of the French Ministry of Foreign Affairs, the support of which, through an ECO-NET program, was extremely appreciated.

References

[1] Landua R 2004 *Phys. Rep.* **403/404** 323
[2] Charlton M 1997 *Hyperfine Interact.* **109** 269
[3] Weber M and Lynn K G 2003 *Principles and Applications of Positron and Positronium Chemistry* ed Y V Jean, P E Mallon and D M Schrader (Singapore: Word Scientific) p 167
[4] Gidley D W, McKinsey D N and Zitzewitz P W 1995 *J. Appl. Phys.* **78** 1406
[5] Van Petegem S, Dauwe C, Van Hoecke T, De Baerdemaeker J and Segers D 2004 *Phys. Rev.* B **70** 115410
[6] Drobychev G, Barysevich A, Delendik K, Karneyeu A, Nédélec P, Sillou D and Voitik O 2006 *J. Nucl. Instrum. Methods* A **567** 290
[7] Paulin R and Ambrosino J 1968 *J. Physique* **29** 263
[8] Shantarovich V P, Suzuki T, Ito Y, Kondo K, Gustov V W, Melikhov I V, Berdonosov S S, Ivanov L N and Yu R S 2007 *Radiat. Phys. Chem.* **76** 257
[9] Delendik K, Emeliantchik I, Litomin A, Rumyantsev V and Voitik O 2003 *Nucl. Phys.* B **125** 394
[10] Kansy J 1996 *J. Nucl. Instrum. Methods* A **374** 235
[11] Palacio C A, De Baerdemaeker J and Dauwe C 2007 Determination of the positron diffusion length in Kapton by analysing the positronium emission *Appl. Surf. Sci.* at press
[12] Brown I W M, Bowden M E, Kemmitt T and MacKenzie K J D 2006 *Curr. Appl. Phys.* **6** 557
[13] Ozaoa R, Ochiai M, Ichimura N, Takahashi H and Inada T 2000 *Thermochim. Acta* **352/353** 91
[14] Kirchner A, MacKenzie K J D, Brown I W M, Kemmitt T and Bowden M E 2006 *J. Membr. Sci.* **87** 264
[15] Goworek T, Ciesielski K, Jasińska B and Wawryszczuk J 1998 *Chem. Phys.* **230** 305
[16] Gidley D W, Frieze W E, Dull T L, Yee A F, Ryan E T and Ho H M 1999 *Phys. Rev.* B **60** R5157
[17] Dauwe C, Consolati G, Kansy J and Van Waeyenberge B 1998 *Phys. Lett.* A **238** 379
[18] Makhov A F 1961 *Sov. Phys.—Solid State* **2** 1934
[19] Brauer G, Anwand W, Nicht E M, Kuriplach J, Procházka I, Bečvář F, Osipowicz A and Coleman P G 2000 *Phys. Rev.* B **62** 5199
[20] Mills A P Jr 1978 *Phys. Rev. Lett.* **41** 1828